

**Modelling runoff from
a Himalayan
debris-covered
glacier**

K. Fujita and A. Sakai

This discussion paper is/has been under review for the journal Hydrology and Earth System Sciences (HESS). Please refer to the corresponding final paper in HESS if available.

Modelling runoff from a Himalayan debris-covered glacier

K. Fujita and A. Sakai

Graduate School of Environmental Studies, Nagoya University, Nagoya, Japan

Received: 16 January 2014 – Accepted: 10 February 2014 – Published: 26 February 2014

Correspondence to: K. Fujita (cozy@nagoya-u.jp)

Published by Copernicus Publications on behalf of the European Geosciences Union.

[Title Page](#)

[Abstract](#)

[Introduction](#)

[Conclusions](#)

[References](#)

[Tables](#)

[Figures](#)

[⏪](#)

[⏩](#)

[◀](#)

[▶](#)

[Back](#)

[Close](#)

[Full Screen / Esc](#)

[Printer-friendly Version](#)

[Interactive Discussion](#)

Abstract

Although the processes by which glacial debris-mantles alter the melting of glacier ice have been well studied, the mass balance and runoff patterns of Himalayan debris-covered glaciers and the response of these factors to climate change are not well understood. Many previous studies have addressed mechanisms of ice melt under debris mantles by applying multiplicative parameters derived from field experiments, and other studies have calculated the details of heat conduction through the debris layer. However, those approaches cannot be applied at catchment scales because debris distributions are heterogeneous and difficult to measure. Here, we establish a runoff model for a Himalayan debris-covered glacier in which the spatial distribution of the thermal properties of the debris mantle is estimated from remotely sensed multi-temporal data. We validated the model for the Tsho Rolpa Glacial Lake–Trambau Glacier basin in the Nepal Himalaya, using hydro-meteorological observations obtained for a 3.5 yr period (1993–1996). We calculated long-term averages of runoff components for the period 1980–2007 using gridded reanalysis datasets. Our calculations suggest that excess meltwater from the debris-covered area contributes significantly to the total runoff, mainly because of its location at lower elevations. Uncertainties in runoff values due to estimations of the thermal properties and albedo of the debris-covered surface were assessed to be approximately 8% of the runoff from the debris-covered area. We evaluated the sensitivities of runoff components to changes in air temperature and precipitation. As expected, warmer air temperatures increase the total runoff by increasing the melting rate; however, increased precipitation slightly reduces the total runoff, as ice melting is suppressed by the increased snow cover and associated high albedo. The response of total runoff to changing precipitation is complex because of the different responses of individual components (glacier, debris, and ice-free terrain) to precipitation levels. The impact of air temperature on inter-annual variability is 23 times greater than that of precipitation.

Modelling runoff from a Himalayan debris-covered glacier

K. Fujita and A. Sakai

[Title Page](#)

[Abstract](#)

[Introduction](#)

[Conclusions](#)

[References](#)

[Tables](#)

[Figures](#)

[⏪](#)

[⏩](#)

[◀](#)

[▶](#)

[Back](#)

[Close](#)

[Full Screen / Esc](#)

[Printer-friendly Version](#)

[Interactive Discussion](#)



1 Introduction

Glaciers are considered to play an important role in the delivery of water resources to densely populated Asian regions (e.g. Cruz et al., 2007). Recent studies have revealed that the response of glaciers to climate variations varies considerably in Asian highland regions (e.g. Fujita and Nuimura, 2011; Bolch et al., 2012; Yao et al., 2012), and that the response depends in part on the characteristics of the debris mantles on Himalayan glaciers. Terminus positions of heavily debris-covered glaciers seem to be insensitive to changes in climate (Scherler et al., 2011), while surface lowering over debris-covered areas seems to be comparable to that in debris-free ablation areas (Nuimura et al., 2011, 2012; Kääb et al., 2012). It is still unclear whether heterogeneity in climatic forcing or debris cover patterns is responsible for observed temporal variations in glacial melt observed in different Himalayan glacier systems. Experimental studies have revealed that thin debris layers accelerate the melting of underlying ice, whereas thick debris layers suppress melting (e.g. Østrem, 1959; Mattson et al., 1993). Some numerical simulations of conductive heat flux through the debris layer have successfully reproduced patterns of ice melting under the debris layer (e.g. Nicholson and Benn, 2006; Reid and Brock, 2010). However, these heat conduction models cannot be applied to basin-scale mass balance calculations in debris-covered glacier systems because the spatial distributions in debris thickness and thermal conductivity are nearly impossible to measure. On the other hand, some hydrological studies in glacierized catchments containing debris-covered glaciers have parameterized ice melting under the debris layer (e.g. Lambrecht et al., 2011; Anderson and Mackintosh, 2012; Immerzeel et al., 2012). Although these studies have been validated by hydrologic and/or other observational data, continuity in surface conditions over time cannot be guaranteed, especially in systems with rapidly changing glaciers. In addition, the debris-covered surfaces of real glaciers exhibit highly heterogeneous and rugged topography, over which no representative thickness is obtainable. Heat absorption in such rugged topography, which includes ice cliffs and supraglacial ponds,

HESSD

11, 2441–2482, 2014

Modelling runoff from a Himalayan debris-covered glacier

K. Fujita and A. Sakai

Title Page

Abstract

Introduction

Conclusions

References

Tables

Figures

⏪

⏩

◀

▶

Back

Close

Full Screen / Esc

Printer-friendly Version

Interactive Discussion

is considered to be one of the significant sources of heat for melting in debris-covered areas (Sakai et al., 2000a, 2002). Therefore, prediction of basin-scale patterns of ice melt on debris-covered glaciers from a simple relationship between debris thickness and ice melting is exceedingly difficult.

To overcome the difficulties discussed above, we have adopted the “thermal resistance” parameter proposed by Nakawo and Young (1982). This parameter is defined as the debris thickness divided by the thermal conductivity of the debris layer and its spatial variations may be obtained from remotely sensed data, such as data obtained from Landsat or ASTER imagery. Nakawo and Rana (1999) used this approach to estimate the distribution of thermal resistance on glaciers from Landsat TM data, and successfully reproduced runoff from the debris-covered Lirung Glacier in the Langtang region of Nepal. Subsequently, Suzuki et al. (2007) demonstrated temporally consistent values of thermal resistance on glaciers in the Bhutan Himalaya, as determined from ASTER data taken on different dates, for which surface temperature and albedo were calibrated using field measurements conducted at the same time as ASTER acquisitions. Zhang et al. (2011, 2012) obtained the thermal resistance distribution of a debris-covered glacier in southeastern Tibet and validated the calculated thermal resistance, melt, and runoff with in situ measurements. However, these studies did not evaluate uncertainties in thermal resistance values, or how these affect both the calculated ice melt under the debris and the resulting runoff. In this study, therefore, our goal was to obtain thermal resistance values and to evaluate uncertainties in the values based on ASTER data acquired in different seasons and years. In addition, we establish an integrated runoff model that incorporates variations in surface conditions, such as debris-covered and debris-free glacier surfaces as well as ice-free terrain. Model performance was tested for a catchment with a debris-covered glacier in the Nepal Himalaya. We evaluate and discuss the uncertainties associated with thermal resistance and albedo, and the sensitivity of runoff to meteorological variables.

Modelling runoff from a Himalayan debris-covered glacier

K. Fujita and A. Sakai

[Title Page](#)

[Abstract](#)

[Introduction](#)

[Conclusions](#)

[References](#)

[Tables](#)

[Figures](#)

[⏪](#)

[⏩](#)

[◀](#)

[▶](#)

[Back](#)

[Close](#)

[Full Screen / Esc](#)

[Printer-friendly Version](#)

[Interactive Discussion](#)



2 Location, data and models

2.1 Delineation and classification of the catchment

We chose as our study site the Tsho Rolpa Glacial Lake–Trambau Glacier basin located at the head of the Rolwaring Valley, in the east Nepal Himalaya (27.9° N, 86.5° E, Fig. 1). Tsho Rolpa (the word “Tsho” means “lake” in the local language) is one of the largest glacial lakes in the Nepal Himalaya. We delineated the basin using a digital elevation model produced from multi-temporal ASTER data (ASTER-GDEM, 2009; Tachikawa et al., 2011). The basin extends from 4500 to 6850 m a.s.l., with a total area of 76.5 km² (Fig. 1a and Table 1).

We divided the surface features of the basin into four categories: debris-covered glacier (debris), debris-free glacier (glacier), ice-free terrain (ground), and lake surface (Tsho Rolpa) to perform the following runoff calculations. Using the clearest available ASTER image acquired on February 2006 (Fig. 1a), we calculated the normalized difference water index (N_W) and normalized difference snow/ice index (N_S) from the following equations:

$$N_W = (r_3 - r_1) / (r_3 + r_1) \quad (1)$$

$$N_S = (r_2 - r_4) / (r_2 + r_4) \quad (2)$$

Here r denotes reflectance of each band (subscript number) in the ASTER sensors. The N_W has been successfully used to delineate glacial lake boundaries in the Himalayas (Fujita et al., 2009). The N_S has been used to evaluate snow cover extent in North America (Hulka, 2008). Thresholds of N_W and N_S are assumed to be 0.42 and 0.94, respectively, to best distinguish the surfaces. Debris-covered surface was visually distinguished from ice-free terrain using surface morphology such as rugged relief and ice flow features (Nagai et al., 2013). Steep slope terrain (steeper than 30°) was also defined as ice-free terrain. The resulting basin surface category map is shown in Fig. 1b, and the hypsometry (area–altitude profile) based on the ASTER-GDEM is shown in Fig. 2.

HESSD

11, 2441–2482, 2014

Modelling runoff from a Himalayan debris-covered glacier

K. Fujita and A. Sakai

Title Page

Abstract

Introduction

Conclusions

References

Tables

Figures

⏪

⏩

◀

▶

Back

Close

Full Screen / Esc

Printer-friendly Version

Interactive Discussion



2.2 Thermal resistance

Thermal resistance is defined as debris thickness divided by the thermal conductivity of the debris layer (Nakawo and Young, 1982). Suzuki et al. (2007) established a methodology to obtain the thermal resistance distribution from ASTER and reanalysis climate data. Zhang et al. (2011) confirmed that the distribution of thermal resistance was well correlated with that of debris thickness from in situ measurements over a southeastern Tibetan glacier with a rather gentle and homogeneous debris-covered surface. We obtained the thermal resistance of the debris-covered area from multi-temporal ASTER data following their methods. The thermal resistance (R_T , m^2KW^{-1}) is defined as:

$$R_T = h/\lambda, \quad (3)$$

where h is debris thickness (m) and λ is thermal conductivity ($\text{Wm}^{-1}\text{K}^{-1}$) of the debris layer. Assuming no heat storage in the debris layer, no heat conduction into temperate glacier ice, and a linear temperature profile within the debris layer, the conductive heat flux through the debris layer (G_d , Wm^{-2}) is described as:

$$G_d = (T_s - T_i)/R_T, \quad (4)$$

where T_s is the surface temperature ($^{\circ}\text{C}$) and T_i the temperature at the interface between debris and ice, which is assumed to be melting point (0°C). The conductive heat flux from the surface toward the debris–ice interface is described as a residual term of the heat balance at the debris surface, according to:

$$G_d = T_s/R_T = (1 - \alpha_d)R_S + R_L - \varepsilon\sigma(T_s + 273.15)^4 + H_S + H_L, \quad (5)$$

where R_S and R_L are the downward short-wave and long-wave radiation fluxes (Wm^{-2}), respectively, H_S and H_L are the sensible and latent turbulent heat fluxes (Wm^{-2}), and α_d is the surface albedo of debris (dimensionless). The debris surface emits

HESSD

11, 2441–2482, 2014

Modelling runoff from a Himalayan debris-covered glacier

K. Fujita and A. Sakai

Title Page

Abstract

Introduction

Conclusions

References

Tables

Figures

⏪

⏩

◀

▶

Back

Close

Full Screen / Esc

Printer-friendly Version

Interactive Discussion



Modelling runoff from a Himalayan debris-covered glacier

K. Fujita and A. Sakai

[Title Page](#)

[Abstract](#)

[Introduction](#)

[Conclusions](#)

[References](#)

[Tables](#)

[Figures](#)

[⏪](#)

[⏩](#)

[◀](#)

[▶](#)

[Back](#)

[Close](#)

[Full Screen / Esc](#)

[Printer-friendly Version](#)

[Interactive Discussion](#)



upward long-wave radiation (W m^{-2}) according to the Stefan–Boltzmann equation with a constant of σ ($5.67 \times 10^{-8} \text{ W m}^{-2} \text{ K}^{-4}$) and surface temperature (T_s), with emissivity (ε , dimensionless) assumed to be 1. All components except for G_d are positive when the fluxes are directed towards the debris surface. Although turbulent heat fluxes have to be taken into account in the exact heat exchange over the debris surface, Suzuki et al. (2007) demonstrated that these fluxes are negligible at Himalayan high elevation because the density of air, the material transferring these fluxes, is approximately half that at sea level. Clear sky conditions, which are required for satellite data utilization, are also associated with a reduced importance of turbulent heat fluxes, especially of latent heat. We therefore assumed that the turbulent heat fluxes were zero ($H_S = H_L = 0$). We can then obtain the thermal resistance at a given point without knowing the debris thickness and thermal conductivity if we know the downward short-wave and long-wave radiation fluxes, the albedo, and the surface temperature. We selected eight cloud-free images of ASTER level 3A1 data, which is a semi-standard ortho-rectified product available from ERSDAC Japan (Table S1). Surface albedo is calculated using three visible near infrared sensors (VNIR; bands 1–3) using the equations described in Yüksel et al. (2008). Surface temperature is obtained from an average of five sensors in the thermal infrared (TIR; bands 10–14) using the formula proposed by Alley and Nilsen (2001). The spatial resolution of the thermal resistance is then constrained by the coarsest resolution of the ASTER TIR sensors (90 m). We utilize NCEP/NCAR reanalysis 6 hourly data (Kalnay et al., 1996) for both downward radiation fluxes at the time (noon) closest to ASTER acquisition.

2.3 Models

2.3.1 Energy and mass balance of debris-covered surface

We calculate heat balance at the debris-covered surface using Eq. (5), but also take into account the turbulent heat fluxes to give results valid for various weather conditions, such as clear, cloudy, rainy, and snowy conditions (although these were

neglected when the thermal resistance was obtained under the clear sky assumption; see Sect. 2.2). The turbulent fluxes are estimated by bulk formulae as:

$$H_S = c_p \rho_a C_d U (T_a - T_s), \quad (6)$$

$$H_L = l_e \rho_a C_d U \tau_w [h_r q(T_a) - q(T_s)], \quad (7)$$

$$\tau_w = e^{-300R_T}, \quad (8)$$

where c_p is the specific heat of air ($1006 \text{ JK}^{-1} \text{ kg}^{-1}$), ρ_a is air density (kg m^{-3}), which depends on elevation, C_d is the bulk coefficient for the debris surface (0.005), U is wind speed (ms^{-1}), T_a is air temperature ($^{\circ}\text{C}$), l_e is the latent heat of evaporation of water ($2.5 \times 10^6 \text{ J kg}^{-1}$), h_r is relative humidity (dimensionless), q is saturated specific humidity (kg kg^{-1}), and τ_w is wetness parameter (dimensionless). Suzuki et al. (2007) revealed that the debris surface was wet ($\tau_w \approx 1$) when its thickness was thin and became exponentially drier ($\tau_w \approx 0$) with increased thermal resistance in the Bhutan Himalaya. Air temperature, solar radiation, relative humidity, and wind speed are required as input variables. Downward long-wave radiation (W m^{-2}) is estimated from an empirical equation using air temperature, relative humidity and the ratio of solar radiation to that at the top of atmosphere based on Glover and McCulloch (1958) and Kondo (1994). We determine the surface temperature that satisfies Eq. (5) by iterative calculation. Once the surface temperature is determined and the heat flux toward the ice–debris interface is positive, the daily melt of ice beneath the debris layer (M_d , $\text{kg m}^{-2} \text{ day}^{-1}$ or mm water equivalent (w.e.) day^{-1}) and then daily runoff water (D_d , mm w.e. day^{-1}) generated at a given point are obtained as:

$$M_d = t_{\text{day}} G_d / l_m, \quad (9)$$

$$D_d = M_d + P_r + \max[H_L / l_e, 0], \quad (10)$$

where t_{day} is the length of a day (86 400 s), l_m is the latent heat of fusion of ice ($3.33 \times 10^5 \text{ J kg}^{-1}$), and P_r is the precipitation that falls as rain (mm w.e. day^{-1}), which is

Modelling runoff from a Himalayan debris-covered glacier

K. Fujita and A. Sakai

Title Page

Abstract

Introduction

Conclusions

References

Tables

Figures

⏪

⏩

◀

▶

Back

Close

Full Screen / Esc

Printer-friendly Version

Interactive Discussion



towards the glacier surface. Turbulent heat fluxes are calculated using the same bulk method given in Eqs. (6) and (7), but using an alternative bulk coefficient for the snow–ice surface (C_s , 0.002, dimensionless) and a constant wetness parameter ($\tau_w = 1$). We determine the surface temperature by iterative calculations, in which the conductive heat flux into the glacier ice is calculated by changing the ice temperature profile. Daily runoff water (D_g , mm w.e. day⁻¹) is obtained as:

$$D_g = t_{\text{day}} Q_g / l_m + P_r + \max[H_L / l_e, 0] - R_f, \quad (14)$$

where R_f is refrozen ice in the snow layer (mm w.e. day⁻¹), which is obtained from the change in the ice temperature profile when surface water is present. All details are described in Fujita and Ageta (2000) and Fujita et al. (2007).

2.3.3 Runoff from ice-free terrain and the lake

Runoff from ice-free terrain is calculated for 50 m elevation bands, based on a simple bucket model proposed by Motoya and Kondo (1999). The potential evaporation rate (E_p , mm w.e. day⁻¹) is obtained from the energy balance:

$$(1 - \alpha_w) R_S + R_L - \varepsilon \sigma (T_s + 273.15)^4 + H_S + H_L = 0, \quad (15)$$

$$\beta E_p = -t_{\text{day}} H_L / l_e = -t_{\text{day}} \rho_a \beta C_t(U) [h_r q(T_a) - q(T_s)], \quad (16)$$

where α_w is the albedo of ice-free terrain (dimensionless), which is assumed to be 0.1, β is the evaporation efficiency (dimensionless), which depends on soil moisture content:

$$\beta = W_a / W_{\text{amax}}, \quad (17)$$

where W_a and W_{amax} are the water content and the maximum water content of surface storage just below the surface, respectively (Fig. S1). Both are expressed in terms of water depth in the surface storage (mm w.e.). The maximum water content is assumed

Modelling runoff from a Himalayan debris-covered glacier

K. Fujita and A. Sakai

Title Page

Abstract

Introduction

Conclusions

References

Tables

Figures

◀

▶

◀

▶

Back

Close

Full Screen / Esc

Printer-friendly Version

Interactive Discussion



to be 5.0 mm w.e. The bulk coefficient (C_t , dimensionless) is parameterized with wind speed (U , ms^{-1}) as:

$$C_t(U) = 0.0027 + 0.0031U. \quad (18)$$

5 Runoff from the ice-free terrain (D_t , mm w.e. day^{-1}) is obtained when the surface storage is full:

$$\max[D_t, 0] = P_r + \max[M_s + \max[H_L/l_e, 0], 0] - \beta E_p - (W_{\text{amax}} - W_a), \quad (19)$$

$$W_n = W_{\text{amax}}, \quad (20)$$

10 where W_n is the water content of the first bucket (mm w.e.) in the next time step (next day). If there is snow cover, snow-melt (M_s) is calculated using Eqs. (11) and (12), in which direct liquid condensation is taken into account if available. If there is no snow, evaporated water (βE_p) is reduced from the rainwater value. Water is first used to fill the surface storage capacity ($W_{\text{amax}} - W_a$) in all cases. If there is insufficient water to fill
 15 the surface storage, no runoff is generated ($D_t = 0$) and the water content in the next time step is given by:

$$W_n = \max[P_r - \beta E_p + W_a, 0]. \quad (21)$$

If evaporation is greater than the sum of rain and water content, evaporated water is constrained by the water in the surface storage ($\beta E_p = W_a$) and no water content is expected in the next time step ($W_n = 0$).

We have little information on the water balance of the Tsho Rolpa Glacial Lake, although the water circulation within the lake has been thoroughly investigated (Sakai et al., 2000b). Therefore we assumed that precipitation would immediately be removed
 25 as runoff from the lake (D_l , mm w.e. day^{-1}), giving the maximum runoff without evaporative loss because the outlet is located just below the lake.

Modelling runoff from a Himalayan debris-covered glacier

K. Fujita and A. Sakai

Title Page

Abstract

Introduction

Conclusions

References

Tables

Figures

⏪

⏩

◀

▶

Back

Close

Full Screen / Esc

Printer-friendly Version

Interactive Discussion



2.3.4 Snow albedo

Snow surface albedo on a given day (dimensionless) is calculated with a scheme proposed by Kondo and Xu (1997), in which an exponential reduction of snow albedo with time after a fresh snowfall is assumed:

$$\alpha_{\text{day}} = (\alpha_{\text{day}-1} - \alpha_f)e^{-1/k} + \alpha_f, \quad (22)$$

where day is the number of days after the latest fresh snow date, which is set to zero (day = 0) when snowfall is greater than 5 mm w.e., and α_f , the albedo of firn, is taken as the minimum snow albedo (0.4, dimensionless). The parameter k depends on air temperature, according to:

$$\begin{aligned} k &= 5.5 - 3.0T_a \quad [T_a < 0.5^\circ\text{C}], \\ k &= 4.0 \quad [T_a \geq 0.5^\circ\text{C}]. \end{aligned} \quad (23)$$

The albedo of the initial fresh snow (day = 0) also depends on air temperature:

$$\begin{aligned} \alpha_0 &= 0.88 \quad [T_a < -1.0^\circ\text{C}], \\ \alpha_0 &= 0.76 - 0.12T_a \quad [-1.0^\circ\text{C} \leq T_a \leq 3.0^\circ\text{C}], \\ \alpha_0 &= 0.40 \quad [T_a > 3.0^\circ\text{C}]. \end{aligned} \quad (24)$$

Surface albedo is affected by the glacier ice or debris surface if the snow layer is thin. According to Giddings and LaChapelle (1961), the penetration of solar radiation into snow is assumed to follow Fick's second law of diffusion with a term for simultaneous absorption, and the surface snow albedo (α_s , dimensionless) over the underlying ice or debris surface is calculated as:

$$\begin{aligned} \alpha_s &= [2 - w(1 - y)]/[2 + w(1 - y)], \\ w &= 2(1 - \alpha_{\text{day}})/(1 + \alpha_{\text{day}}), \\ y &= [2 - 2\alpha_b - w(1 + \alpha_b)]e^{-Kx}/[-w(1 + \alpha_b)\cosh Kx - 2(1 - \alpha_b)\sinh Kx], \end{aligned} \quad (25)$$

Modelling runoff from a Himalayan debris-covered glacier

K. Fujita and A. Sakai

Title Page

Abstract

Introduction

Conclusions

References

Tables

Figures

◀

▶

◀

▶

Back

Close

Full Screen / Esc

Printer-friendly Version

Interactive Discussion

where K is the extinction coefficient of snow (30 m^{-1} ; Greuell and Konzelmann, 1994), x is the depth of the snow layer (m), and α_b is the albedo of the underlying surface (dimensionless), which is taken to be ice (α_i) or debris (α_d) based on the targets. The albedo of glacier ice (α_i) is assumed to be 0.2 based on our field observations on Asian glaciers (Takeuchi and Li, 2008; Fujita et al., 2011).

2.3.5 Bucket model calculating river runoff

All water generated over the debris-covered part (D_d), debris-free snow or ice (D_g), ice-free terrain (D_t) and the lake (D_l) is added to the river system through two types of storage, internal and ground storages (Motoya and Kondo, 1999). A schematic diagram that also includes the surface storage for ice-free terrain is shown in Fig. S1. The surface water inflows (D_d , D_g , D_t , D_l) are added to the internal storage. Outflow from the internal storage (F_b , mm w.e. day^{-1}) will occur and be directly added to the final runoff when the volume of water stored (W_b , mm w.e.) exceeds the maximum capacity ($W_{b\text{max}}$, 500 mm w.e.) according to:

$$F_b = F_a - (W_{b\text{max}} - W_b) \quad (26)$$

where F_a is the total inflow into the internal storage, which is made up of the individual surface water inflows (D_d , D_g , D_t , D_l). Leakage from the internal storage (F_c , mm w.e. day^{-1}) is simultaneously calculated as:

$$F_c = k_b W_b, \quad (27)$$

where k_b is a leak rate parameter assumed to be 0.3 (dimensionless). It implies that 30% of the internally stored water will be lost in a day. Part of the leakage from the internal storage will be directly added to the final runoff and the rest will flow into the ground storage (W_c , mm w.e.). There is no limit on the capacity of the ground storage. Leakage from the ground storage (F_d , mm w.e. day^{-1}) is given by:

$$F_d = k_c W_c, \quad (28)$$

where k_c is a leak rate parameter assumed to be 0.03 (dimensionless). This flow will form the continuous basal flow of the river system. We obtain the final runoff (F_f , mm w.e. day⁻¹) as:

$$F_f = F_b + r_c F_c + F_d. \quad (29)$$

The fraction (r_c , dimensionless) is assumed to be 0.8. The final runoff can be calculated for individual runoffs from the debris-covered surface (R_d), the debris-free glacier (R_g), the ice-free terrain (R_t), and the lake (R_l). We summarize these runoffs by considering a debris grid with 90 m resolution and the hypsometry of the debris-free glacier surface and ice-free terrain in 50 m elevation bands (Fig. 2).

2.3.6 Probability of snow and rain

Precipitation across the Himalayan regions takes place mainly during the summer monsoon season so that the precipitation phase (snowfall or rainfall) has to be taken into account. Based on observational reports in Tibet (Ueno et al., 1994; Sakai et al., 2006a), we assume the probability of snowfall (P_s , mm w.e.) and rainfall (P_r , mm w.e.) to depend on air temperature as follows:

$$P_s = P_p \quad [T_a \leq 0.0^\circ\text{C}],$$

$$P_s = (1 - T_a/4.0)P_p \quad [0.0^\circ\text{C} < T_a < 4.0^\circ\text{C}],$$

$$P_s = 0 \quad [T_a \geq 4.0^\circ\text{C}], \quad (30)$$

$$P_r = P_p - P_s \quad (31)$$

where P_p is daily precipitation (mm w.e.).

2.4 Meteorological and hydrological data

Meteorological, hydrological, and limnological observations were conducted in the 1990s (Fig. S2; Yamada, 1998; Sakai et al., 2000b). The observations are used

Modelling runoff from a Himalayan debris-covered glacier

K. Fujita and A. Sakai

[Title Page](#)

[Abstract](#)

[Introduction](#)

[Conclusions](#)

[References](#)

[Tables](#)

[Figures](#)

[⏪](#)

[⏩](#)

[◀](#)

[▶](#)

[Back](#)

[Close](#)

[Full Screen / Esc](#)

[Printer-friendly Version](#)

[Interactive Discussion](#)

to confirm the plausibility of the gridded data and to validate the calculated runoff, for which we use gridded data as model inputs to examine the long-term mean and seasonal cycle of runoff components. Air temperature, solar radiation, relative humidity, and wind speed are taken from the NCEP/NCAR reanalysis gridded data (NCEP-1, Kalnay et al., 1996). Air temperature at the elevation of the observation site (4540 m a.s.l.) is linearly interpolated from air temperatures at geopotential heights of 500 and 600 hPa; the temperature lapse rate is also obtained from these data. Wind speed at a 2 m height from the surface (U , ms^{-1}) is estimated from 10 m wind in the reanalysis data (U_{10} , ms^{-1}), based on the assumption of a logarithmic dependence of wind speed on height:

$$U = U_{10} \left[\ln(2.0/z_0) / \ln(10.0/z_0) \right], \quad (32)$$

where surface roughness z_0 is assumed to be 0.1 m. The ground-based Aphrodite daily precipitation data are used, which have a spatial resolution of $0.5^\circ \times 0.5^\circ$ (Yatagai et al., 2009). All variables except for wind speed show significant correlations between gridded and observational data (Fig. S3). Air temperature shows a particularly high linear correlation, with little bias. Although solar radiation, relative humidity, and wind speed show less significant or no correlations, Fujita and Ageta (2000) have pointed out that uncertainties in these variables are less important for the mass balance of Tibetan glaciers than those of air temperature and precipitation. Precipitation directly affects both glacier mass balance and runoff (Fujita et al., 2007) but pentad (5 day) data do show a significant correlation (Fig. S3). We therefore use the gridded data for all variables except for precipitation, and compare modelled and observed runoffs to find the best set of calibration coefficients using the Aphrodite precipitation data and elevation gradient of precipitation (Sect. 3.2).

3 Results

3.1 Distributions of thermal resistance and albedo

We calculated the distribution of thermal resistance from eight ASTER images (Figs. S4 and S5). Some images showed a plausible distribution of thermal resistance (Fig. S4) but a fragmented distribution was obtained in winter images (Fig. S5). Because the ice–debris interface is assumed to be at the melting point temperature in the calculation of thermal resistance (T_i in Eq. 4), it may not be possible to calculate the thermal resistance under cold winter conditions. We therefore obtain an average distribution of the thermal resistance from the four plausible distributions as shown in Fig. 1b. Where calculations were not possible for the debris-covered part, as shown by grey shading in Fig. 1b and at higher elevations, zero thermal resistance is assumed, implying a debris-free glacier.

Comparisons of individual thermal resistances against the average show some degree of variability (Fig. 3a). A linear regression of standard deviation against the average suggests that the thermal resistance has an uncertainty of 30 % (Fig. 3c). We simultaneously obtain a distribution of surface albedo, which is required to calculate the thermal resistance and complete the energy mass balance model of the debris-covered surface. Although one image taken in October 2004 shows rather large scatter (Fig. 3b), the uncertainty in albedo expressed as a standard deviation is of a similar level to that of thermal resistance (Fig. 3d). We evaluate the influences of these uncertainties on runoff from the debris-covered surface later (Sect. 4.1).

3.2 Validation

A one-year cycle of the calculation runs from 1 October to 30 September of the next year. We first conducted a four-year calculation from 1 October 1992 to 30 September 1996, and compared the results with the observed runoff at the outlet of the Tsho Rolpa Glacial Lake (shown as a yellow cross in Fig. 1a). Because the

HESSD

11, 2441–2482, 2014

Modelling runoff from a Himalayan debris-covered glacier

K. Fujita and A. Sakai

Title Page

Abstract

Introduction

Conclusions

References

Tables

Figures

⏪

⏩

◀

▶

Back

Close

Full Screen / Esc

Printer-friendly Version

Interactive Discussion



times greater than from the debris-free glacier surface or ice-free terrain, which both have runoff height slightly less than that due to precipitation because of evaporative loss. The similar runoff heights of debris-free glacier surface and ice-free terrain suggest that the entire debris-free glacier is in a steady state (Table 1).

4 Discussion

4.1 Uncertainty

In earlier work on thermal resistance, Suzuki et al. (2007) calibrated surface temperature and albedo with field measurements performed at the same time as ASTER acquisitions in the Bhutan Himalaya. In the present study, however, we have no in situ data for the calibration so that the reanalysis data are used without adjustment. Our thermal resistances have greater scatter than those of Suzuki et al. (2007, Fig. 5) probably because uncalibrated data were used. On the other hand, Zhang et al. (2011, 2012) obtained the thermal resistance distribution of a debris-covered glacier in southeastern Tibet from a single ASTER image. They validated the thermal resistance, melt, and runoff calculations with their in situ measurements of debris thickness, melt rate, and runoff, respectively. However, these studies did not evaluate how the uncertainty of thermal resistance affects the calculated melt under the debris or the resulting runoff. We therefore calculated the influence of uncertainties in thermal resistance and albedo (Fig. 3c and d). At some points there are insufficient data to calculate the standard deviation of thermal resistance, so for such points we use an estimate from the linear regression (Fig. 3c). The standard deviation of the albedo was obtained for all points so that the regression curve was not used (Fig. 3d). We obtain the runoff anomaly (dR) from the control calculation in Sect. 3.3 by averaging positive and negative cases according to:

$$dR(v) = [R(v + \delta_v) - R(v - \delta_v)] / 2, \quad (33)$$

Modelling runoff from a Himalayan debris-covered glacier

K. Fujita and A. Sakai

Title Page

Abstract

Introduction

Conclusions

References

Tables

Figures

⏪

⏩

◀

▶

Back

Close

Full Screen / Esc

Printer-friendly Version

Interactive Discussion



Modelling runoff from a Himalayan debris-covered glacier

K. Fujita and A. Sakai

Title Page

Abstract

Introduction

Conclusions

References

Tables

Figures

⏪

⏩

◀

▶

Back

Close

Full Screen / Esc

Printer-friendly Version

Interactive Discussion

where ν and δ_ν denote the parameter used for the control calculation (thermal resistance or albedo) and its standard deviation, respectively. Changes in albedo ($R_{T_{ave}}$, $d\alpha$) or thermal resistance (dR_T , α_{ave}) reduce the debris runoff (Table 2). Uncertainty due to albedo (-8%) has a slightly larger effect than that due to thermal resistance (-5%). The simultaneous change of both parameters (dR_T , $d\alpha$) results in an additive impact on the debris runoff (-14%). Combinations in which the two parameters are changed in different directions ($+\delta R_T$ and $-\delta\alpha$ / $-\delta R_T$ and $+\delta\alpha$) suggest that the uncertainty due to albedo has more effect on the debris runoff than that due to thermal resistance. In the absence of calibration data, the use of multiple ASTER images to derive thermal resistance and albedo gives a runoff uncertainty within 8% .

4.2 Effects of debris cover, lake and glacier

It is clear that the debris-covered area is supplying significant excess meltwater to the total runoff (Table 1 and Fig. 6). Elevation profiles of debris-covered and debris-free surfaces suggest comparable runoffs from both surfaces (Fig. 7a), so that the significant excess meltwater may be attributed to the lower elevation of the debris-covered area (Fig. 2). To evaluate whether the excess meltwater is generated by accelerated melt due to thinner and darker debris cover or by the lower elevation of the debris-covered area, we performed a sensitivity calculation by assuming no debris cover (the no debris assumption in Table 2). Compared with the control calculation, a debris-free surface would yield slightly less water (-3%), implying that the significant excess water is generated mainly by the lower elevation of the debris-covered area, and is slightly increased by the acceleration effect of thin and dark debris. This is the opposite of that estimated for the Lirung Glacier in the Langtang region, Nepal (Nakawo and Rana, 1999), where the debris cover significantly suppressed the melting of ice underneath. In fact, the regional distribution of thermal resistance suggested that the debris cover over the Trambau Glacier was thinner than that over the other glaciers in the Khumbu and neighbouring regions (Suzuki et al., 2007).

Modelling runoff from a Himalayan debris-covered glacier

K. Fujita and A. Sakai

[Title Page](#)

[Abstract](#)

[Introduction](#)

[Conclusions](#)

[References](#)

[Tables](#)

[Figures](#)

[⏪](#)

[⏩](#)

[◀](#)

[▶](#)

[Back](#)

[Close](#)

[Full Screen / Esc](#)

[Printer-friendly Version](#)

[Interactive Discussion](#)

Another topographic feature of the basin is the Tsho Rolpa Lake, one of the largest glacial lakes in the Nepal Himalaya. In our calculation the lake dimensions are assumed to be constant, but the lake has expanded since the 1950s at a rate of $0.03 \text{ km}^2 \text{ yr}^{-1}$ (Yamada, 1998; Komori et al., 2004; Sakai et al., 2009b). We therefore performed another sensitivity calculation without a lake. The thermal resistance ($0.0151 \text{ m}^2 \text{ KW}^{-1}$), albedo (0.230) and elevation (4560 m a.s.l.) over the lake are taken from values at the lowermost part of the debris-covered area (approximately 500 m from the glacier terminus). Runoff from the debris-covered surface and the lake significantly increases by 22 % from the control (Table 2). This suggests that ice located at a lower elevation is the main source of excess meltwater in the basin, and the meltwater might have decreased with expansion of the lake.

Glaciers are recognized as water resources in the Asian highlands. The disappearance of glaciers is projected to result in severe depletion of river water that will threaten human life (e.g. Cruz et al., 2007). In this regard, the contribution of glacier meltwater to river runoff has been evaluated in a number of studies (e.g. Immerzeel et al., 2010; Kaser et al., 2010). However, considering that precipitation could be still expected over the terrain after the glaciers disappear, the reduction in glaciers would not directly result in such a severe depletion of river runoff. A future projection for a Himalayan catchment demonstrated that increased precipitation and seasonal snow melt would compensate for the decrease in glacier meltwater (Immerzeel et al., 2012). We therefore simply assumed that runoff height over the ice-free terrain (941 mm) was applicable to the whole basin and then evaluated the runoff under the no ice environment (Table 3). Because the excess meltwater is added to the control total runoff, the no ice assumption results in a significant runoff reduction of 43 %. Although an increase in evaporation, which is expected under the climatic conditions resulting in the disappearance of a glacier, is not taken into account, river water will still be available from the basin. In terms of future water availability, more uncertainty will be caused by projected changes in precipitation.

4.3 Sensitivities

To understand how the basin consisting of debris-covered glaciers responds to changes in climatic variables such as air temperature and precipitation, we calculated the runoff sensitivities by altering the annual air temperature and precipitation, by $\pm 0.1^\circ\text{C}$ for air temperature or $\pm 10\%$ for precipitation from the control conditions. The runoff anomaly is obtained in the same way as uncertainty (Sect. 4.1), by averaging positive and negative cases for which signs are taken into account (Eq. 33). Warmer air temperature significantly increases melting of ice over both debris-covered and debris-free surfaces and thus total runoff, while increased evaporative water loss over the ice-free terrain is negligible (Table 4). Elevation profiles of response to the warming show no significant difference between debris-covered and debris-free surface at a given elevation (Fig. 7b). The doubled sensitivity of runoff height over the debris-covered area should be attributed to its lower elevation as discussed in Sect. 4.2 (Table 4). Because the debris-free glacier surface mainly consists of the high accumulation zone reaching to above 6000 m a.s.l., warming will have a limited impact overall. On the other hand, an increase in precipitation will potentially prolong the duration of high albedo snow cover, which suppresses absorption of solar radiation, and will result in a runoff reduction from ice, while runoff from the ice-free terrain and the lake will increase with precipitation (Table 4). These opposing responses compensate for each other and thus result in a smaller influence on total runoff than that caused by warming. The elevation profiles of response show greater sensitivity over the debris-free glacier than over the debris-covered ice, which may be caused by different albedo settings for glacier ice and debris (Fig. 7b). These sensitivities to changes in air temperature and precipitation cannot simply be compared directly. Considering the standard deviations of air temperature (0.47°C) and precipitation (97 mm, 9.4 %) for the period 1979–2007 (28 yr), we obtain the variability in runoff associated with the variability in climatic variables (Table 4). It is clear that variability of the total runoff caused by air temperature variability is 23 times greater than that caused by precipitation variability.

The small changes applied above simply result in a linear response, but we further tested runoff sensitivity to precipitation by changing the precipitation over a wider range, from 40 to 200 % of that used in the control calculation. Runoffs from the ice-free terrain and the lake respond linearly to changing precipitation in proportion to their areas, while those from debris-covered and debris-free surfaces respond non-linearly (Fig. 8a). In particular, a deficit of precipitation will yield extreme ice melt because it gives a dark surface without snow cover (blue line in Fig. 8a). Glacier runoff will become stable under conditions of extreme humidity because of compensation between suppressed ice melting and increased rain water. Summing components with different sensitivities results in a complicated total runoff response (black line in Fig. 8a). This suggests that present climatic and topographic conditions of the target basin have the smallest sensitivity to changing precipitation. If the precipitation regime changes significantly for a long period of time, runoff would respond more significantly than under the present regime though the glacier extent would also change with time. Seasonal cycles of runoff under the two extreme conditions (50 % and 200 % of the control) show impressive responses (Fig. 8b). A wetter climate simply increases the runoff during the humid monsoon season, which is affected by precipitation seasonality (blue line in Fig. 8b) while a drier climate significantly alters the seasonal cycle of runoff (orange line in Fig. 8b). Reduced precipitation will accelerate ice melting in the spring as the dark ice surface uncovered by high albedo snow. Although such an effect may not be obvious in the sensitivity obtained by changing precipitation over a small range ($\pm 10\%$ for instance), a change in precipitation could potentially alter the seasonality of runoff, which is important for regional water availability (e.g. Kaser et al., 2010).

5 Conclusions

We have developed an integrated runoff model, in which the energy–water–mass balance is calculated over different surfaces such as debris-covered surface, debris-free glacier and ice-free terrain. To take into account the effect of debris on ice melt,

HESSD

11, 2441–2482, 2014

Modelling runoff from a Himalayan debris-covered glacier

K. Fujita and A. Sakai

[Title Page](#)

[Abstract](#)

[Introduction](#)

[Conclusions](#)

[References](#)

[Tables](#)

[Figures](#)

[⏪](#)

[⏩](#)

[◀](#)

[▶](#)

[Back](#)

[Close](#)

[Full Screen / Esc](#)

[Printer-friendly Version](#)

[Interactive Discussion](#)



Modelling runoff from a Himalayan debris-covered glacier

K. Fujita and A. Sakai

[Title Page](#)[Abstract](#)[Introduction](#)[Conclusions](#)[References](#)[Tables](#)[Figures](#)[⏪](#)[⏩](#)[◀](#)[▶](#)[Back](#)[Close](#)[Full Screen / Esc](#)[Printer-friendly Version](#)[Interactive Discussion](#)

5 other glaciers, which have higher thermal resistance, may suppress more strongly the ice melt beneath the debris. Therefore, further study is required on whether the excess meltwater found over the Trambau Glacier is also found over other glaciers. Despite the few observational data for validation, our approach may be applicable to a larger scale if multiple ASTER data are available. However, the settings for precipitation (ratio to reanalysis data and elevation gradient) will be the main source of uncertainty.

10 Sensitivity analysis showed that the total runoff was 23 times more sensitive to change in air temperature than to change in precipitation when their inter-annual variability was taken into account (Table 4). Change in precipitation affects runoffs from the ice (both debris-covered and debris-free) and the ice-free terrain in opposing directions. Increased precipitation suppresses ice melting through the high albedo of snow cover whereas runoff from ice-free terrain increases with precipitation. The two effects compensate each other, so that the response of the total runoff is smaller than that for changes in air temperature (Table 4). Although a small but negative response of total runoff was derived for a small perturbation of precipitation, the potential response to change in precipitation could be complicated for a large perturbation (Fig. 8a). In particular, a deficit of precipitation could alter the seasonal cycle of runoff (Fig. 8b).

15 Other studies calculating heat conduction through a debris layer have accurately reproduced the melt rate of ice beneath the debris mantle if its thickness and conductivity are known (Nicholson and Benn, 2006; Reid and Brock, 2010). Even for a single glacier, however, the distributions of debris thickness and thermal conductivity are unobtainable because of the heterogeneously rugged surface of debris-covered areas. In this regard, our approach using thermal resistance is a practical solution to calculate the ice melting under the debris cover on a wider scale, such as a basin or region. The assumption of a linear temperature profile within the debris layer may cause large uncertainty in both deriving thermal resistance and calculating ice melt. In particular, this linear approximation is unrealistic when the debris layer is too thick. Although the thermal resistance method has been successfully applied to glaciers with thinner debris as demonstrated by Zhang et al. (2011, 2012) or in this study, further

research is required to understand whether this method can be applied to thicker debris layers or whether any modifications are required.

Supplementary material related to this article is available online at
<http://www.hydrol-earth-syst-sci-discuss.net/11/2441/2014/hessd-11-2441-2014-supplement.pdf>.

Acknowledgements. This study is supported by the Funding Program for Next Generation World-Leading Researchers (NEXT Program).

References

- Alley, R. E. and Nilsen, M. J.: Algorithm theoretical basis document for brightness temperature version 3.1, Jet Propulsion Laboratory, 14 pp., Pasadena, USA, 2001.
- Anderson, B. and Mackintosh, A.: Controls on mass balance sensitivity of maritime glaciers in the southern Alps, New Zealand: the role of debris cover, *J. Geophys. Res.*, 117, F01003, doi:10.1029/2011JF002064, 2012.
- ASTER-GDEM: available at: <http://gdem.ersdac.jspacesystems.or.jp/> (last access: 20 December 2013), 2009.
- Berthier, E. and Vincent, C.: Relative contribution of surface mass-balance and ice-flux changes to the accelerated thinning of Mer de Glace, French Alps, over 1979–2008, *J. Glaciol.*, 58, 501–512, doi:10.3189/2012JoG11J083, 2012.
- Bolch, T., Kulkarni, A., Kääb, A., Huggel, C., Paul, F., Cogley, J. G., Frey, H., Kargel, J. S., Fujita, K., Scheel, M., Bajracharya, S., and Stoffel, M.: The state and fate of Himalayan glaciers, *Science*, 336, 310–314, doi:10.1126/science.1215828, 2012.
- Cruz, R. V., Harasawa, H., Lal, M., Wu, S., Anokhin, Y., Punsalmaa, B., Honda, Y., Jafari, M., Li, C., and Huu Ninh, N.: Asia, in: *Climate Change 2007: Impacts, Adaptation and Vulnerability, Contribution of Working Group II to the Fourth Assessment Report of the Intergovernmental Panel on Climate Change*, edited by: Parry, M. L., Canziani, O. F., Palutikof, J. P., van der Linden, P. J., and Hanson, C. E., Cambridge University Press, Cambridge, UK, 469–506, 2007.

Modelling runoff from a Himalayan debris-covered glacier

K. Fujita and A. Sakai

Title Page

Abstract

Introduction

Conclusions

References

Tables

Figures



Back

Close

Full Screen / Esc

Printer-friendly Version

Interactive Discussion



Modelling runoff from a Himalayan debris-covered glacier

K. Fujita and A. Sakai

Title Page

Abstract

Introduction

Conclusions

References

Tables

Figures

⏪

⏩

◀

▶

Back

Close

Full Screen / Esc

Printer-friendly Version

Interactive Discussion

Fujita, K. and Ageta, Y.: Effect of summer accumulation on glacier mass balance on the Tibetan Plateau revealed by mass-balance model, *J. Glaciol.*, 46, 244–252, doi:10.3189/172756500781832945, 2000.

Fujita, K. and Nuimura, T.: Spatially heterogeneous wastage of Himalayan glaciers, *P. Natl. Acad. Sci. USA*, 108, 14011–14014, doi:10.1073/pnas.1106242108, 2011.

Fujita, K., Sakai, A., and Chhetri, T. B.: Meteorological observation in Langtang Valley, Nepal Himalayas, 1996, *Bull. Glacier Res.*, 15, 71–78, 1997.

Fujita, K., Ohta, T., and Ageta, Y.: Characteristics and climatic sensitivities of runoff from a cold-type glacier on the Tibetan Plateau, *Hydrol. Process.*, 21, 2882–2891, doi:10.1002/hyp.6505, 2007.

Fujita, K., Sakai, A., Nuimura, T., Yamaguchi, S., and Sharma, R. R.: Recent changes in Imja Glacial Lake and its damming moraine in the Nepal Himalaya revealed by in situ surveys and multi-temporal ASTER imagery, *Environ. Res. Lett.*, 4, 045205, doi:10.1088/1748-9326/4/4/045205, 2009.

Fujita, K., Takeuchi, N., Nikitin, S. A., Surazakov, A. B., Okamoto, S., Aizen, V. B., and Kubota, J.: Favorable climatic regime for maintaining the present-day geometry of the Gregoriev Glacier, Inner Tien Shan, *The Cryosphere*, 5, 539–549, doi:10.5194/tc-5-539-2011, 2011.

Giddings, J. C. and LaChapelle, E.: Diffusion theory applied to radiant energy distribution and albedo of snow, *J. Geophys. Res.*, 66, 181–189, doi:10.1029/JZ066i001p00181, 1961.

Glover, J. and McCulloch, G.: The empirical relation between solar radiation and hours of sunshine, *Q. J. Roy. Meteor. Soc.*, 84, 172–175, 1958.

Greuell, W. and Konzelmann, T.: Numerical modelling of the energy balance and the englacial temperature of Greenland Ice Sheet, Calculations for the ETH-Camp location (West Greenland, 1155 m.a.s.l.), *Global Planet. Change*, 9, 91–114, doi:10.1016/0921-8181(94)90010-8, 1994.

Hulka, J.: Calibrating ASTER for snow cover analysis, in: 11th AGILE International Conference on Geographic Information Science 2008, University of Girona, Spain, available at: http://itcnt05.itc.nl/agile_old/Conference/2008-Girona/PDF/63_DOC.pdf (last access: 19 December 2013), 2008.

Immerzeel, W., van Beek, L. P. H., and Bierkens, M. F. P.: Climate change will affect the Asian water towers, *Science*, 328, 1382–1385, doi:10.1126/science.1183188, 2010.

Modelling runoff from a Himalayan debris-covered glacier

K. Fujita and A. Sakai

Title Page

Abstract

Introduction

Conclusions

References

Tables

Figures

⏪

⏩

◀

▶

Back

Close

Full Screen / Esc

Printer-friendly Version

Interactive Discussion

- Immerzeel, W., van Beek, L. P. H., Konz, M., Shrestha, A. B., and Bierkens, M. F. P.: Hydrological response to climate change in a glacierized catchment in the Himalayas, *Climatic Change*, 110, 721–736, doi:10.1007/s10584-011-0143-4, 2012.
- 5 Kääb, A., Berthier, E., Nuth, C., Gardelle, J., and Arnaud, Y.: Contrasting patterns of early twenty-first-century glacier mass change in the Himalayas, *Nature*, 488, 495–498, doi:10.1038/nature11324, 2012.
- Kalnay, E., Kanamitsu, M., Kistler, R., Collins, W., Deaven, D., Gandin, L., Iredell, M., Saha, S., White, G., Woollen, J., Zhu, Y., Chelliah, M., Ebisuzaki, W., Higgins, W., Janowiak, J., Mo, K. C., Ropelewski, C., Wang, J., Leetmaa, A., Reynolds, R., Jenne, R., and Joseph, D.: The NCEP/NCAR 40 year reanalysis project, *B. Am. Meteorol. Soc.*, 77, 437–471, 1996.
- 10 Kaser, G., Großhauser, M., and Marzeion, B.: Contribution potential of glaciers to water availability in different climate regimes, *P. Natl. Acad. Sci. USA*, 107, 20223–20227, doi:10.1073/pnas.1008162107, 2010.
- Komori, J., Gurung, D. R., Iwata, S., and Yabuki, H.: Variation and lake expansion of Chubda Glacier, Bhutan Himalayas, during the last 35 years, *Bull. Glaciol. Res.*, 21, 49–55, 2004.
- Kondo, J.: *Meteorology of the Water Environment-Water and Heat Balance of the Earth's Surface*, Asakura Shoten Press, Tokyo, 1994 (in Japanese).
- Kondo, J. and Xu, J.: Seasonal variations in the heat and water balances for nonvegetated surfaces, *J. Appl. Meteorol.*, 36, 1676–1695, doi:10.1175/1520-0450(1997)036<1676:SVITHA>2.0.CO;2, 1997.
- 20 Lambrecht, A., Mayer, C., Hagg, W., Popovnin, V., Rezepkin, A., Lomidze, N., and Svanadze, D.: A comparison of glacier melt on debris-covered glaciers in the northern and southern Caucasus, *The Cryosphere*, 5, 525–538, doi:10.5194/tc-5-525-2011, 2011.
- Mattson, L. E., Gardner, J. S., and Young, G. J.: Ablation on debris covered glaciers: an example from the Rakhiot Glacier, Punjab, Himalaya, *Int. Assoc. Hydrol. Sci. Publ.*, 218, 289–296, 1993.
- 25 Motoya, K. and Kondo, J.: Estimating the seasonal variations of snow water equivalent, runoff and water temperature of a stream in a basin using the new bucket model, *J. Jpn. Soc. Hydrol. Water Resour.*, 12, 391–407, 1999.
- 30 Nagai, H., Fujita, K., Nuimura, T., and Sakai, A.: Southwest-facing slopes control the formation of debris-covered glaciers in the Bhutan Himalaya, *The Cryosphere*, 7, 1303–1314, doi:10.5194/tc-7-1303-2013, 2013.

Modelling runoff from a Himalayan debris-covered glacier

K. Fujita and A. Sakai

[Title Page](#)

[Abstract](#)

[Introduction](#)

[Conclusions](#)

[References](#)

[Tables](#)

[Figures](#)

[⏪](#)

[⏩](#)

[◀](#)

[▶](#)

[Back](#)

[Close](#)

[Full Screen / Esc](#)

[Printer-friendly Version](#)

[Interactive Discussion](#)

- Nakawo, M. and Rana, B.: Estimate of ablation rate of glacier ice under a supraglacial debris layer, *Geogr. Ann. A*, 81, 695–701, 1999.
- Nakawo, M. and Young, G. J.: Estimate of glacier ablation under a debris layer from surface temperature and meteorological variables, *J. Glaciol.*, 28, 29–34, 1982.
- 5 Nash, J. E. and Sutcliffe, J. V.: River flow forecasting through conceptual models part I – A discussion of principles, *J. Hydrol.*, 10, 282–290, doi:10.1016/0022-1694(70)90255-6, 1970.
- Nicholson, L. and Benn, D. I.: Calculating ice melt beneath a debris layer using meteorological data, *J. Glaciol.*, 52, 463–470, doi:10.3189/172756506781828584, 2006.
- 10 Nuimura, T., Fujita, K., Fukui, K., Asahi, K., Aryal, R., and Ageta, Y.: Temporal changes in elevation of the debris-covered ablation area of Khumbu glacier in the Nepal Himalaya since 1978, *Arct. Antarct. Alp. Res.*, 43, 246–255, doi:10.1657/1938-4246-43.2.246, 2011.
- Nuimura, T., Fujita, K., Yamaguchi, S., and Sharma, R. R.: Elevation changes of glaciers revealed by multitemporal digital elevation models calibrated by GPS survey in the Khumbu region, Nepal Himalaya, 1992–2008, *J. Glaciol.*, 58, 648–656, doi:10.3189/2012JoG11J061, 2012.
- 15 Østrem, G.: Ice melting under a thin layer of moraine and the existence of ice cores in moraine ridges, *Geogr. Ann. A*, 41, 228–230, 1959.
- Reid, T. D. and Brock, B. W.: An energy-balance model for debris-covered glaciers including heat conduction through the debris layer, *J. Glaciol.*, 56, 903–916, doi:10.3189/002214310794457218, 2010.
- 20 Sakai, A., Takeuchi, N., Fujita, K., and Nakawo, M.: Role of supraglacial ponds in the ablation processes of a debris-covered glacier in the Nepal Himalayas, *Int. Assoc. Hydrol. Sci. Publ.*, 264, 119–130, 2000a.
- 25 Sakai, A., Chikita, K., and Yamada, T.: Expansion of a moraine-dammed glacier lake, Tsho Rolpa, in Rolwaling Himal, Nepal Himalaya, *Limnol. Oceanogr.*, 45, 1401–1408, doi:10.4319/lo.2000.45.6.1401, 2000b.
- Sakai, A., Nakawo, M., and Fujita, K.: Distribution characteristics and energy balance of Ice cliffs on debris-covered glaciers, Nepal Himalaya, *Arct. Antarct. Alp. Res.*, 34, 12–19, 2002.
- 30 Sakai, A., Matsuda, Y., Fujita, K., Matoba, S., Uetake, J., Satow, K., Duan, K., Pu, J., Nakawo, M., and Yao, T.: Meteorological observation at 1 July Glacier in northwest China from 2002 to 2005, *Bull. Glaciol. Res.*, 23, 23–31, 2006a.

Modelling runoff from a Himalayan debris-covered glacier

K. Fujita and A. Sakai

[Title Page](#)

[Abstract](#)

[Introduction](#)

[Conclusions](#)

[References](#)

[Tables](#)

[Figures](#)

[⏪](#)

[⏩](#)

[◀](#)

[▶](#)

[Back](#)

[Close](#)

[Full Screen / Esc](#)

[Printer-friendly Version](#)

[Interactive Discussion](#)

- Sakai, A., Fujita, K., Duan, K., Pu, J., Nakawo, M., and Yao, T.: Five decades of shrinkage of 1 July Glacier, Qilian Shan, China, *J. Glaciol.*, 52, 11–16, doi:10.3189/172756506781828836, 2006b.
- Sakai, A., Fujita, K., Nakawo, M., and Yao, T.: Simplification of heat balance calculation and its application to the glacier runoff from the 1 July Glacier in northwest China since the 1930s, *Hydrol. Process.*, 23, 585–596, doi:10.1002/hyp.7187, 2009a.
- Sakai, A., Nishimura, K., Kadota, T., and Takeuchi, N.: Onset of calving at supraglacial lakes on debris covered glaciers of the Nepal Himalayas, *J. Glaciol.*, 55, 909–917, doi:10.3189/002214309790152555, 2009b.
- Sakai, A., Fujita, K., Narama, C., Kubota, J., Nakawo, M., and Yao, T.: Reconstructions of annual discharge and equilibrium line altitude of glaciers at Qilian Shan, northwest China, from 1978 to 2002, *Hydrol. Process.*, 24, 2798–2806, doi:10.1002/hyp.7700, 2010.
- Scherler, D., Bookhagen, B., and Strecker, M. R.: Spatially variable response of Himalayan glaciers to climate change affected by debris cover, *Nat. Geosci.*, 4, 156–159, doi:10.1038/ngeo1068, 2011.
- Seko, K.: Seasonal variation of altitudinal dependence of precipitation in Langtang valley, Nepal Himalayas, *Bull. Glacier Res.*, 5, 41–47, 1987.
- Suzuki, R., Fujita, K., and Ageta, Y.: Spatial distribution of the thermal properties on debris-covered glaciers in the Himalayas derived from ASTER data, *Bull. Glaciol. Res.*, 24, 13–22, 2007.
- Tachikawa, T., Hato, M., Kaku, M., and Iwasaki, A.: Characteristics of ASTER GDEM version 2, *Int. Geosci. Remote Se.*, 3657–3660, 2011.
- Takeuchi, N. and Li, Z.: Characteristics of surface dust on Ürümqi glacier No. 1 in the Tien Shan mountains, China, *Arct. Antarct. Alp. Res.*, 40, 744–750, 2008.
- Ueno, K., Endoh, N., Ohata, T., Yabuki, H., Koike, M., Ohta, T., and Zhang, Y.: Characteristics of precipitation distribution in Tanggula, Monsoon, 1993, *Bull. Glacier Res.*, 12, 39–46, 1994.
- Yamada, T.: Lake and its outburst flood in the Nepal Himalaya, Monograph No. 1, *Data C. Glacier Res.*, Jpn. Soc. Snow Ice, Tokyo, 96 pp., 1998.
- Yao, T., Thompson, L., Yang, W., Yu, W., Gao, Y., Guo, X., Yang, X., Duan, K., Zhao, H., Xu, B., Pu, J., Lu, A., Xiang, Y., Kattel, D. B., and Joswiak, D.: Different glacier status with atmospheric circulations in Tibetan Plateau and surroundings, *Nature Clim. Change*, 2, 663–667, doi:10.1038/nclimate1580, 2012.

Modelling runoff from a Himalayan debris-covered glacier

K. Fujita and A. Sakai

Title Page

Abstract

Introduction

Conclusions

References

Tables

Figures

⏪

⏩

◀

▶

Back

Close

Full Screen / Esc

Printer-friendly Version

Interactive Discussion

Yatagai, A., Arakawa, O., Kamiguchi, K., Kawamoto, H., Nodzu, M. I., and Hamada, A.: A 44 year daily gridded precipitation dataset for Asia based on a dense network of rain gauges, SOLA, 5, 137–140, doi:10.2151/sola.2009-035, 2009.

5 Yüksel, A., Akay, A. E., and Gudogan, R.: Using ASTER imagery in land use/cover classification of eastern Mediterranean landscapes according to CORINE land cover project, Sensors, 8, 1237–1251, doi:10.3390/s8021287, 2008.

Zhang, Y., Fujita, K., Liu, S., Liu, Q., and Nuimura, T.: Distribution of debris thickness and its effect on ice melt at Hailuogou Glacier, southeastern Tibetan Plateau, using in situ surveys and ASTER imagery, J. Glaciol., 57, 1147–1157, doi:10.3189/002214311798843331, 2011.

10 Zhang, Y., Hirabayashi, Y., and Liu, S.: Catchment-scale reconstruction of glacier mass balance using observations and global climate data: case study of the Hailuogou catchment, south-eastern Tibetan Plateau, J. Hydrol., 444–445, 146–160, doi:10.1016/j.jhydrol.2012.04.014, 2012.

15 Zhang, G., Kang, S., Fujita, K., Huintjes, E., Xu, J., Yamazaki, T., Haginoya, S., Yang, W., Scherer, D., Schneider, C., and Yao, T.: Energy and mass balance of the Zhadang Glacier surface, central Tibetan Plateau, J. Glaciol., 59, 137–148, doi:10.3189/2013JoG12J152, 2013.

Modelling runoff from a Himalayan debris-covered glacier

K. Fujita and A. Sakai

Table 2. Uncertainty in runoff due to thermal resistance (R_T) and albedo (α), and topographical assumptions of debris-covered area of the Trambau Glacier. Influences are obtained by averaging mass balance anomalies from positive and negative cases (Eq. 33 in Sect. 4.1). Combinations of changes in both parameters in different directions were also tested ($+\delta R_T$ and $-\delta\alpha$ / $-\delta R_T$ and $+\delta\alpha$). Errors represent inter-annual variability calculated for the period 1979–2007 (28 yr).

Difference from control	Annual runoff (million m ³)	Change in percent (%)	Annual runoff height (mm)
$R_{T_{ave}}, d\alpha$	-5.9 ± 1.0	-8.5	-511 ± 87
dR_T, α_{ave}	-3.6 ± 0.2	-5.2	-315 ± 17
Both change (dTR, d α)	-9.5 ± 1.2	-13.6	-820 ± 101
$+\delta R_T$ and $-\delta\alpha$	2.7 ± 0.8	3.9	237 ± 73
$-\delta R_T$ and $+\delta\alpha$	-1.7 ± 0.7	-2.4	-145 ± 60
No debris assumption	-2.0 ± 2.9	-2.9	-172 ± 254
Control (debris)	69.7 ± 6.1	(100.0)	6030 ± 529
No lake assumption*	15.5 ± 0.6	21.8	1183 ± 49
Control (debris + lake)*	70.8 ± 6.2	(100.0)	5420 ± 476

* Control variables for the no lake assumption are the summations of debris and lake.

[Title Page](#)
[Abstract](#)
[Introduction](#)
[Conclusions](#)
[References](#)
[Tables](#)
[Figures](#)
[⏪](#)
[⏩](#)
[◀](#)
[▶](#)
[Back](#)
[Close](#)
[Full Screen / Esc](#)
[Printer-friendly Version](#)
[Interactive Discussion](#)

Modelling runoff from a Himalayan debris-covered glacier

K. Fujita and A. Sakai

Table 3. Annual runoff and runoff height associated with the presence of ice in the Tsho Rolpa Glacial Lake–Trambau Glacier basin. Errors represent inter-annual variability calculated for the period 1979–2007 (28 yr).

	Annual runoff (million m ³)	Contribution (%)	Annual runoff height (mm)
No ice assumption	71.9 ± 7.1	57.3	941 ± 93
Control (total)	125.5 ± 12.7	100.0	1641 ± 166
Difference	−60.2	−42.7	−788
Precipitation	78.5 ± 7.3	62.6	1027 ± 96

[Title Page](#)
[Abstract](#)
[Introduction](#)
[Conclusions](#)
[References](#)
[Tables](#)
[Figures](#)
[Back](#)
[Close](#)
[Full Screen / Esc](#)
[Printer-friendly Version](#)
[Interactive Discussion](#)

Modelling runoff from a Himalayan debris-covered glacier

K. Fujita and A. Sakai

[Title Page](#)

[Abstract](#)

[Introduction](#)

[Conclusions](#)

[References](#)

[Tables](#)

[Figures](#)

[⏪](#)

[⏩](#)

[◀](#)

[▶](#)

[Back](#)

[Close](#)

[Full Screen / Esc](#)

[Printer-friendly Version](#)

[Interactive Discussion](#)

Table 4. Sensitivities of annual runoff (million m^3) and runoff height (mm) (parentheses) associated with changes in air temperature (dT_a , 0.1°C) and precipitation (dP_p , 10 % or 97 mm) for the Tsho Rolpa Glacial Lake–Trambau Glacier basin. Also shown are sensitivities associated with inter-annual variability (δ , standard deviation) of air temperature and precipitation calculated for the period 1979–2007 (28 yr).

	dT_a (per 0.1°C)	dP_p (per 10%)	δT_a (0.47°C)	δP_p (9.4 %, 97 mm)
Total	3.5 (45)	−0.8 (−10)	16.4 (215)	−0.7 (−10)
Glacier	1.9 (67)	−3.1 (−110)	9.0 (315)	−2.9 (−103)
Debris	1.6 (139)	−1.2 (−101)	7.6 (656)	−1.1 (−95)
Ground	−0.03 (−1)	3.4 (97)	−0.2 (−5)	3.2 (92)
Lake	0.0 (0)	0.1 (76)	0.0 (0)	0.1 (72)

Modelling runoff from a Himalayan debris-covered glacier

K. Fujita and A. Sakai

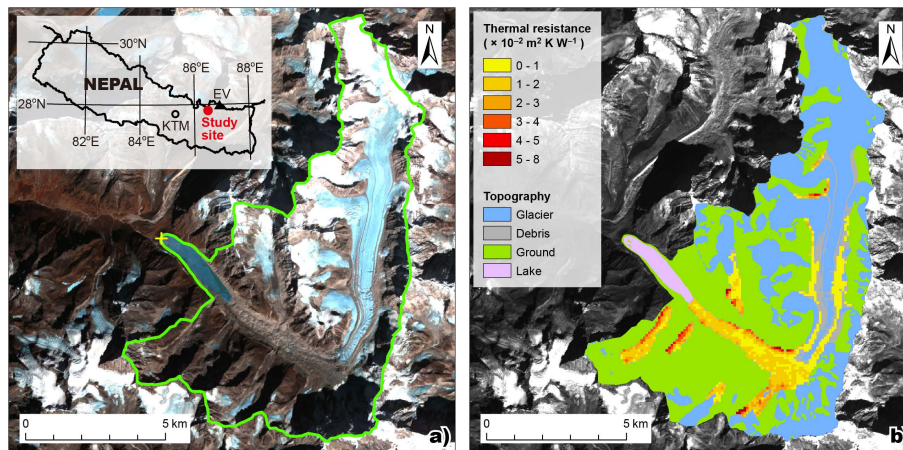


Fig. 1. Tsho Rolpa Glacial Lake–Trambau Glacier basin. **(a)** Catchment (green line) and **(b)** categorized surface features with thermal resistance of debris cover. Inset box shows locations of Kathmandu (KTM), Mt. Everest (EV), and the study site. Average thermal resistance is superimposed on the debris-covered area where available. Yellow cross in **(a)** denotes the location at which meteorological and hydrological observations were conducted in the 1990s. The background image is ASTER data taken in February 2006.

Title Page

Abstract

Introduction

Conclusions

References

Tables

Figures

⏪

⏩

◀

▶

Back

Close

Full Screen / Esc

Printer-friendly Version

Interactive Discussion

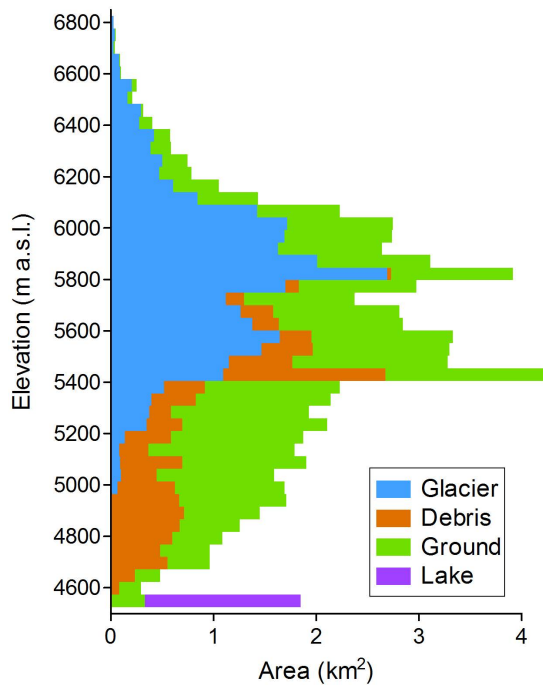


Fig. 2. Hypsometry of the Tsho Rolpa Glacial Lake–Trambau Glacier basin categorized by surface features (Fig. 1b).

Modelling runoff from a Himalayan debris-covered glacier

K. Fujita and A. Sakai

Title Page

Abstract Introduction

Conclusions References

Tables Figures

⏪ ⏩

◀ ▶

Back Close

Full Screen / Esc

Printer-friendly Version

Interactive Discussion



Modelling runoff from a Himalayan debris-covered glacier

K. Fujita and A. Sakai

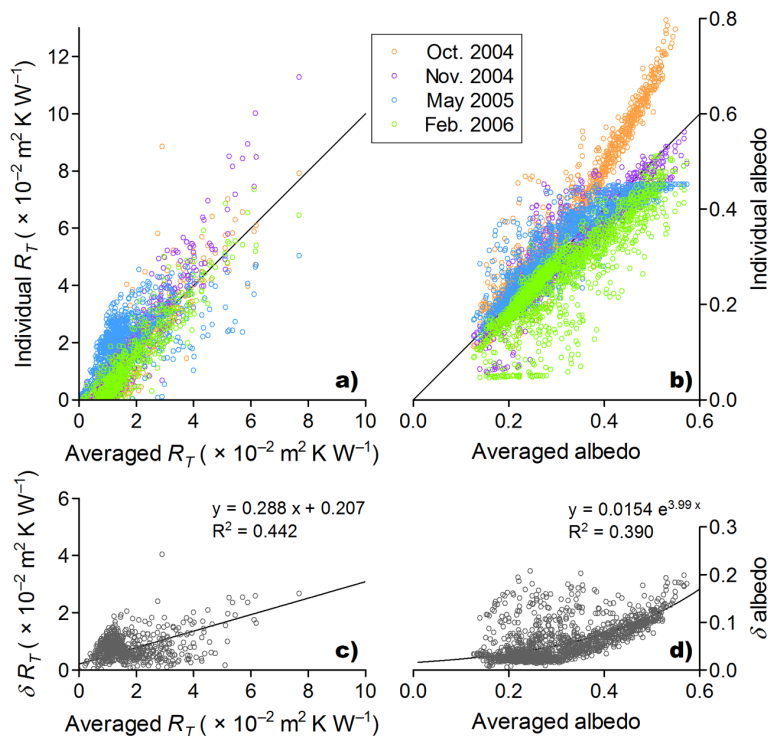


Fig. 3. Scattergrams of **(a)** thermal resistance (R_T) and **(b)** albedo of multi-temporal ASTER data against their averages, which are used to calculate ice melting under the debris-covered surface of the Trambau Glacier. Also shown are standard deviations (δ) of **(c)** thermal resistance (R_T) and **(d)** albedo.

[Title Page](#)
[Abstract](#)
[Introduction](#)
[Conclusions](#)
[References](#)
[Tables](#)
[Figures](#)
[◀](#)
[▶](#)
[◀](#)
[▶](#)
[Back](#)
[Close](#)
[Full Screen / Esc](#)
[Printer-friendly Version](#)
[Interactive Discussion](#)

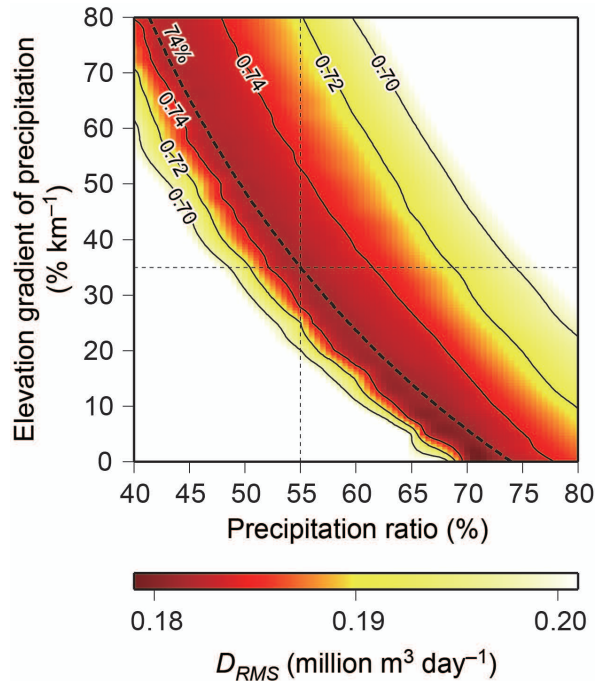


Fig. 4. Root mean square difference (D_{RMS} ; color shading) and Nash–Sutcliffe model efficiency coefficient (contour lines) of the model performance for the Tsho Rolpa Glacial Lake–Trambau Glacier basin calculated for the period 1993–1996 (location shown as yellow cross in Fig. 1a), as a function of precipitation ratio (horizontal axis) against the original Aphrodite precipitation and elevation gradient of precipitation (vertical axis). We adopt 55% as the precipitation ratio and $35\% \text{ km}^{-1}$ as the elevation gradient of precipitation for subsequent analysis (thin dashed lines). The thick dashed line denotes the 74% precipitation ratio isoline for the whole basin.

Modelling runoff from a Himalayan debris-covered glacier

K. Fujita and A. Sakai

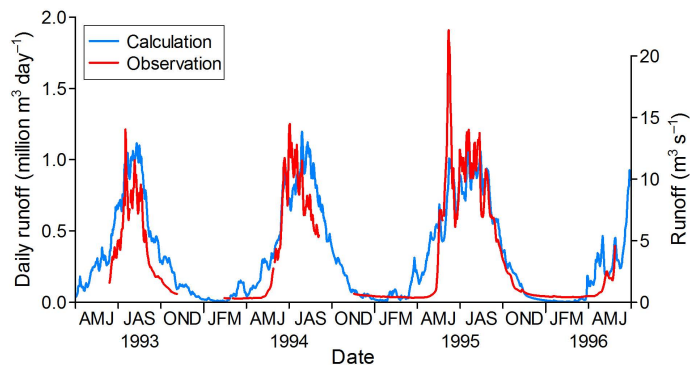


Fig. 5. Observed and calculated runoff at the outlet of the Tsho Rolpa Glacial Lake–Trambau Glacier basin for the period 1993–1996 (location shown as yellow cross in Fig. 1a).

[Title Page](#)[Abstract](#)[Introduction](#)[Conclusions](#)[References](#)[Tables](#)[Figures](#)[⏪](#)[⏩](#)[◀](#)[▶](#)[Back](#)[Close](#)[Full Screen / Esc](#)[Printer-friendly Version](#)[Interactive Discussion](#)

Modelling runoff from a Himalayan debris-covered glacier

K. Fujita and A. Sakai

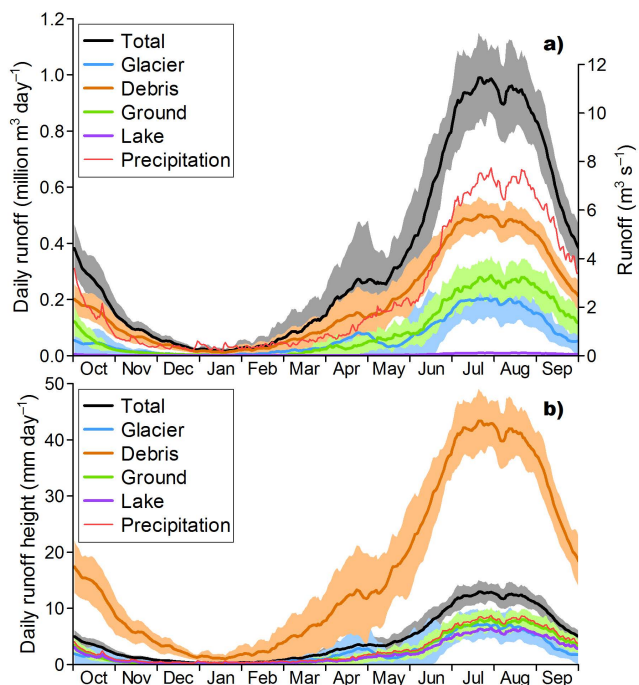


Fig. 6. Seasonal cycles of **(a)** daily runoff and **(b)** daily runoff height of the Tsho Rolpa Glacial Lake–Trambau Glacier basin calculated for the period 1979–2007 (28 yr). Shading denotes inter-annual variability obtained for the same period. The inter-annual variability of runoff height from the lake is not shown for better visibility in **(b)**. Also shown is the seasonal cycle of precipitation averaged for the whole basin (thin red lines).

Modelling runoff from a Himalayan debris-covered glacier

K. Fujita and A. Sakai

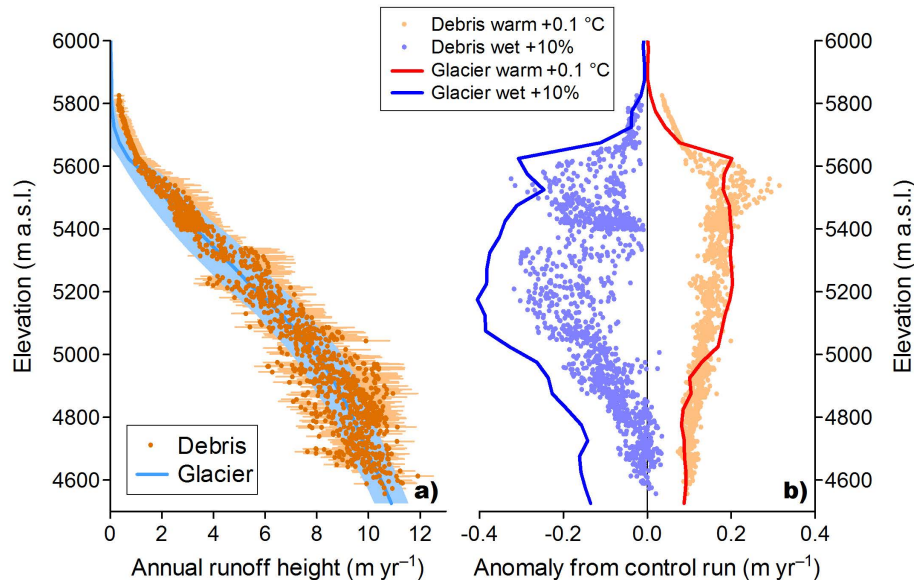


Fig. 7. Elevation profiles of (a) annual runoff height over debris-free glacier (Glacier) and debris-covered (Debris) surfaces, and of (b) responses under conditions of warming (air temperature increase 0.1 °C) and wetting (precipitation increase 10 %) of the Trambau Glacier calculated for the period 1979–2007 (28 yr). Shading and error bars in (a) denote inter-annual variability for the same period.

[Title Page](#)
[Abstract](#)
[Introduction](#)
[Conclusions](#)
[References](#)
[Tables](#)
[Figures](#)
[⏪](#)
[⏩](#)
[◀](#)
[▶](#)
[Back](#)
[Close](#)
[Full Screen / Esc](#)
[Printer-friendly Version](#)
[Interactive Discussion](#)

Modelling runoff from a Himalayan debris-covered glacier

K. Fujita and A. Sakai

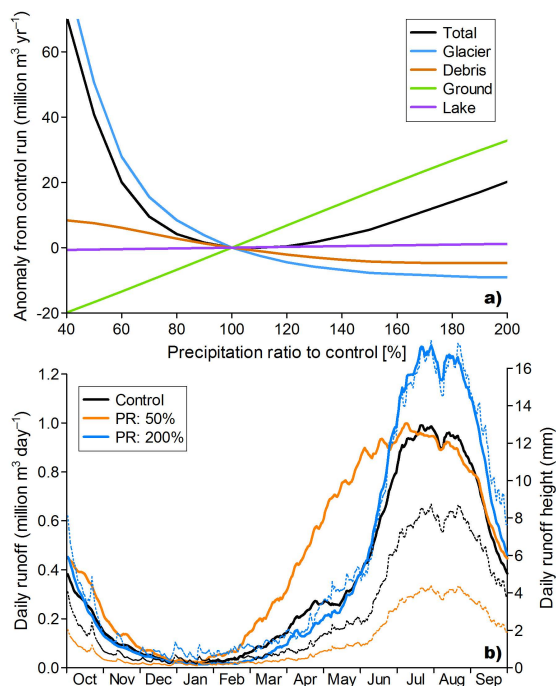


Fig. 8. (a) Response of annual runoffs to changing precipitation ratio against the control condition and (b) seasonal cycles of total runoff (thick lines) and precipitation (thin dotted lines) in the two extreme cases of the Tsho Rolpa Glacial Lake–Trambau Glacier basin calculated for the period 1979–2007 (28 yr). Response in (a) is described by the anomaly with respect to the control calculation.